21st century trends in Antarctic temperature and polar stratospheric cloud (PSC) area in the GEOS chemistry-climate model

M. M. Hurwitz[1] and P. A. Newman[2]

Received 16 October 2009; revised 21 May 2010; accepted 3 June 2010; published 7 October 2010.

[1] This study examines trends in Antarctic temperature and A_{PSC}, a temperature proxy for the area of polar stratospheric clouds, in an ensemble of Goddard Earth Observing System (GEOS) chemistry-climate model (CCM) simulations of the 21st century. A selection of greenhouse gas, ozone-depleting substance, and sea surface temperature scenarios is used to test the trend sensitivity to these parameters. One scenario is used to compare temperature trends in two versions of the GEOS CCM. An extended austral winter season is examined in detail. In May, June, and July, the expected future increase in CO_2-related radiative cooling drives temperature trends in the Antarctic lower stratosphere. At 50 hPa, a 1–3 K cooling is expected between 2000 and 2100. Ozone levels increase, despite this robust cooling signal and the consequent increase in A_{PSC}, suggesting the enhancement of stratospheric transport in future. In the lower stratosphere, the choice of climate change scenarios does not affect the magnitude of the early winter cooling. Midwinter temperature trends are generally small. In October, A_{PSC} trends have the same sign as the prescribed halogen trends. That is, there are negative A_{PSC} trends in "realistic future" simulations, where halogen loading decreases in accordance with the Montreal Protocol and CO_2 continues to increase. In these simulations, the speed of ozone recovery is not influenced by either the choice of sea surface temperature and greenhouse gas scenarios or by the model version.

Citation: Hurwitz, M. M., and P. A. Newman (2010), 21st century trends in Antarctic temperature and polar stratospheric cloud (PSC) area in the GEOS chemistry-climate model, *J. Geophys. Res.*, *115*, D19109, doi:10.1029/2009JD013397.

1. Introduction

[2] The stratosphere cooled in the late 20th and early 21st century [*Randel et al.*, 2009]. This recent stratospheric cooling has been attributed to increasing greenhouse gas concentrations [*Ramaswamy et al.*, 2001 and 2006] and, in the polar lower stratosphere where the largest decreases in temperature have been observed, to ozone depletion [*Ramaswamy et al.*, 2001; *Manzini et al.*, 2003]. In the Antarctic, stratospheric cooling has been most evident in late winter and spring: The breakup date of the Southern Hemisphere (SH) polar vortex has been delayed in recent decades, due to the radiative cooling associated with springtime ozone depletion [*Akiyoshi et al.*, 2009].

[3] *Eyring et al.* [2007] evaluated chemistry-climate model (CCM) simulations of the 21st century using boundary conditions representing a "realistic future" in which atmospheric CO_2 concentrations continue to increase while compliance with the Montreal Protocol leads to decreased halogen loading. The vertical profile of the predicted global and annual mean cooling was consistent with increasing atmospheric greenhouse gas concentrations. Midwinter polar temperature trends (January–February in the Northern Hemisphere, NH; August–September in the SH) varied widely between models in the NH and were generally negative but not statistically significant in the SH.

[4] Previous studies have examined the relationship between polar stratospheric temperature and polar ozone. *Rex et al.* [2004 and 2006] found a linear, empirical relationship between chemical ozone loss and V_{PSC} (a high-latitude temperature integral representing the volume of polar stratospheric clouds, PSCs) in Arctic winters. Similarly, *Tilmes et al.* [2007] found a compact, linear relationship between ozone loss and the potential for chlorine activation (PACl, a combined measure of stratospheric chlorine and temperature), in a chemistry-climate simulation of the late 20th century. While the linearity of the relationship between ozone loss and measures of the wintertime-averaged potential for ozone depletion may not persist in the future [*Braesicke et al.*, 2006], polar stratospheric temperature may remain an important indicator of the potential for chemical ozone loss. For example, *Newman et al.* [2004] predicted that, in the early 21st century, halogen-related decreases in the size of the Antarctic ozone hole

[1]NASA Postdoctoral Program, NASA Goddard Space Flight Center, Greenbelt, Maryland, USA.
[2]NASA Goddard Space Flight Center, Greenbelt, Maryland, USA.

Copyright 2010 by the American Geophysical Union.
0148-0227/10/2009JD013397

Table 1. GEOS CCM Simulations Used in the Analysis[a]

Simulation	GEOS CCM	Analysis Period	GHG Scenario	SST and Sea Ice Fields	ODS Scenario
V1 F1	V1	1996–2099	A1b	HadGEM1	WMO Ab
V1 F2	V1	1971–2049	A1b	HadGEM1	WMO Ab
V1 F3	V1	1971–2052	A1b	NCAR CCSM 2.0 A1b	WMO Ab
V1 F4	V1	2000–2099	A1b	NCAR CCSM 3.0 A1b	WMO Ab
V1 F5	V1	2000–2099	A2	NCAR CCSM 3.0 A2	WMO Ab
V2 F4	V2	2000–2099	A1b	NCAR CCSM 3.0 A1b	WMO Ab
Cl60	V1	1960–2099	A1b	NCAR CCSM 3.0 A1b	"low chlorine": fixed at 1960 levels
WA	V1	1974–2075	A1b	1974–2049: NCAR CCSM 2.0; 2050–2075: NCAR CCSM 3.0	"world avoided": V1 F3 with increasing chlorine

[a]NCAR, National Center for Atmospheric Research; CCSM 3.0, Community Climate System Model version 3; WMO, World Meteorological Association; HadGEM1, Hadley Centre Global Environmental Model version 1.

could be partially offset by increases in ozone hole size related to greenhouse gas–related cooling.

[5] *Hitchcock et al.* [2009] evaluated the conditions necessary for PSC formation in "realistic past" and "realistic future" simulations using the Canadian Middle Atmosphere Model (CMAM). "A_{PSC}" was defined as the polar stratospheric area with temperatures below a fixed temperature threshold for the formation of nitric acid trihydrate particles (i.e., the "cold area," typically ~195 K at 50 hPa [see *Kawa et al.*, 1997]). The A_{PSC} threshold was held constant throughout the 21st century, since it was determined that predicted changes in water vapor and nitric acid would have a negligible impact on the temperature threshold for PSC formation in future. In the lower stratosphere, increased greenhouse gas concentrations should lead to cooling (i.e., increased A_{PSC}), whereas recovery of the ozone layer should lead to warming (i.e., decreased A_{PSC}, due to decreasing levels of stratospheric halogens). In the Antarctic, *Hitchcock et al.* [2009] found that May–December-averaged A_{PSC} remained fairly constant throughout the 21st century, balancing increased A_{PSC} in the autumn and early winter with decreased A_{PSC} in spring.

[6] This study examines Antarctic temperature and A_{PSC} trends for an extended austral winter season, spanning from May to October, in an ensemble of Goddard Earth Observing System (GEOS) chemistry-climate model (CCM) simulations of the 21st century. In section 2, two versions of the GEOS CCM and a set of eight simulations are briefly described. These simulations use a variety of climate change and ozone depletion/recovery scenarios, allowing the relative impact of sea surface temperatures (SSTs), greenhouse gases, and ozone-depleting substances (ODSs) on polar temperature trends to be evaluated.

[7] A_{PSC} and polar cap temperature trends are quantified in section 3. In this study, "A_{PSC}" is defined as the area at 50 hPa where temperatures are equal to or less than 195 K. Defined as such, A_{PSC} is a simple diagnostic that can be calculated at any desired time interval and without defining a fixed winter season, for the region in which chemical ozone depletion can potentially occur. A_{PSC} trends in the GEOS CCM are compared with the CMAM results [*Hitchcock et al.*, 2009]. Also, two versions of the GEOS CCM are compared, using one of the "realistic future" scenarios. Radiative and statistical calculations are used to attribute the A_{PSC} trends to changes in CO_2 and ODSs. Section 3 closes by examining the impact of these trends on polar ozone. Section 4 summarizes the main findings.

2. Model Description

[8] Eight Goddard Earth Observing System (GEOS) chemistry-climate model (CCM) simulations will be used to investigate temperature and A_{PSC} trends in the future stratosphere. These simulations consider a range of future emissions scenarios for greenhouse gases (GHGs) and for ozone-depleting substances (as summarized in Table 1).

[9] The GEOS version 1 (V1) CCM couples the GEOS-4 general circulation model (GCM) with a comprehensive stratospheric chemistry module [*Bloom et al.*, 2005; *Pawson et al.*, 2008]. The GEOS V1 CCM has 2° latitude × 2.5° longitude horizontal resolution and 55 vertical levels, with a model top at 0.01 hPa. Predicted distributions of water vapor, ozone, greenhouse gases (CO_2, CH_4, and N_2O) and CFCs (CFC-11 and CFC-12) feedback to the radiative calculations. The GEOS V1 CCM was included in the *Eyring et al.* [2007] evaluation of 21st century CCM simulations and has been since used to investigate future changes in the stratospheric age of air [*Oman et al.*, 2009], upper stratospheric ozone [*Oman et al.*, 2010], the distribution of ozone in the post-CFC era [*Li et al.*, 2009], and the impact of climate change on the annual mean ozone recovery [*Waugh et al.*, 2009].

[10] Most of the GEOS V1 CCM simulations are forced with scenario A1b for well-mixed greenhouse gas emissions, increasing to ~710 ppmv CO_2 by 2100 [*IPCC*, 2002], as shown in Table 1. Simulation V1 F5 is forced with emissions scenario A2 (~850 ppmv CO_2 by 2100).

[11] Sea surface temperatures (SSTs) and sea ice concentrations from a Hadley Centre Global Environmental Model version 1 (HadGEM1) simulation [*Johns et al.*, 2006] were prescribed in the V1 F1 and V1 F2 simulations. Two integrations from the National Center for Atmospheric Research Community Climate System Model version 3 [*Collins et al.*, 2006] provided boundary conditions for the remaining simulations.

[12] The *World Meteorological Association* (*WMO*) [2003] Ab time series of surface concentrations of ozone-depleting substances (ODSs) is used in five of the GEOS V1 CCM simulations (see Table 1). In the present study, equivalent effective stratospheric chlorine (EESC), total inorganic chlorine loading plus 60 times the total inorganic

Table 2. 2000–2099 Antarctic Polar Cap Temperature Trends at 50 hPa[a]

	ΔCO_2 (ppmv)	ΔEESC (ppbv)	May	June	July	August	September	October
V1 F1	345	−2.5	**−14.8** ± 7.0	**−19.8** ± 8.6	**−19.1** ± 13.2	−9.4 ± 22.6	16.7 ± 28.2	**80.7** ± 39.8
V1 F4	345	−2.5	**−25.7** ± 7.8	**−27.0** ± 8.8	**−20.0** ± 12.8	−12.6 ± 22.6	2.7 ± 37.2	**44.1** ± 40.6
V1 F5	485	−2.5	**−27.9** ± 8.2	**−27.5** ± 9.2	**−14.4** ± 12.0	1.9 ± 21.2	4.9 ± 31.4	29.1 ± 36.4
V2 F4	345	−2.5	**−8.4** ± 4.8	**−10.1** ± 5.8	**−8.0** ± 7.2	−6.9 ± 10.4	6.3 ± 14.2	**45.2** ± 22.6
Cl60	345	0	**−19.4** ± 6.8	**−25.5** ± 9.0	**−38.2** ± 14.6	**−49.8** ± 30.8	**−44.2** ± 39.8	−32.0 ± 35.6

[a]10^{-3} K a^{-1}. Trends that are statistically significant at the 95% confidence level or higher are denoted in bold. Errors denote 2 standard deviations.

bromine at 1 hPa, is used to quantify the amount of ODSs in the stratosphere. V1 simulations F1, F2, F3, F4, and F5 represent a "realistic future" in which ODS levels decrease relatively monotonically through the 21st century (2.8 ppbv EESC in 2050) and where stratospheric ozone concentrations recover to 1980 levels in the mid-21st century [*Eyring et al.*, 2007]. Two more ODS scenarios are also considered in the present study. In the Cl60 ("low chlorine") simulation, chlorine is fixed at 1960 levels, and thus, no ozone hole develops. The WA ("world avoided") simulation considers a scenario in which CFCs remained unregulated. In the WA scenario, EESC increases steadily from the 1970s to 29.6 ppbv by 2050 [*Newman et al.*, 2009]. Volcanic and solar cycle forcings are not considered in any of the simulations; also, the GEOS V1 CCM includes neither an internally generated quasi-biennial oscillation (QBO) in zonal winds nor a forced QBO.

[13] Version 2 (V2) of the GEOS CCM is based on the GEOS-5 atmospheric GCM. As described by *Rienecker et al.* [2008], the GEOS-4 and GEOS-5 GCMs use essentially the same advection and gravity wave drag schemes; however, GEOS-5 uses a new set of physics parameterizations, with upgraded radiative transfer and convective components. The stratospheric chemistry component in the GEOS V2 CCM is essentially the same as in the GEOS V1 CCM [see *Pawson et al.*, 2008]. The GEOS V2 CCM has 72 vertical levels but the same horizontal resolution (2° × 2.5°) as the GEOS V1 CCM model. *Hurwitz et al.* [2010] conducted a brief evaluation of the stratospheric dynamics and chemistry in the GEOS V2 CCM using a "reference past" simulation of the late twentieth century, in which both greenhouse gases and EESC increase with time. The GEOS V2 CCM performed well, except for two deficiencies common to many CCMs: the late breakup of the Antarctic vortex and the overprediction of total ozone. This is the first publication to consider V2 simulation F4, a "realistic future" simulation with the same boundary conditions as V1 F4. This particular simulation lacks water vapor feedback to the radiation, potentially biasing temperatures in the Antarctic stratosphere.

3. Results

3.1. Antarctic A_{PSC} and Polar Cap Temperature Trends

[14] This section examines polar cap temperature and A_{PSC} trends in the Antarctic stratosphere in a set of GEOS CCM simulations of the 21st century (see Table 1). Modeled 3-D monthly mean temperature fields are used to investigate (1) the seasonal dependence of A_{PSC} and temperature trends and (2) the trend sensitivity to the GHG, SST, and ODS boundary conditions and to the model version used. Temperature trends for the polar cap (poleward of 60°S) are shown in Tables 2 (50 hPa; T_{50hPa}) and 3 (10 hPa; T_{10hPa}). In Tables 2 and 3, trends are shown for each month and for each simulation, where data are available for the whole period. Linear trends are computed using a least squares technique. The statistical significance of the trends is calculated by resampling the temperature time series [*Efron*, 1979]. For reference, the approximate differences in atmospheric CO_2 concentration and in EESC at 1 hPa, between 2000 and 2099, are also shown.

[15] In the autumn and early winter, the Antarctic lower stratosphere cools between 2000 and 2099. T_{50hPa} trends are negative and statistically significant in all simulations in May, June, and July (Table 2). With the exception of Cl60, temperature trends are small and are not statistically significant in August and September. In October, T_{50hPa} trends diverge as a result of trends in EESC: positive trends in three of the realistic future simulations (V1 F1, V1 F4, and V2 F4), trends not significantly different from zero in Cl60 and V1 F5, and a large and negative trend in WA (for 2000–2075; not shown).

[16] An A_{PSC} diagnostic is calculated for each of the GEOS CCM simulations (Table 1), by summing the areas at all longitudes and polar latitudes where the temperature is

Table 3. 2000–2099 Antarctic Polar Cap Temperature Trends at 10 hPa[a]

	ΔCO_2 (ppmv)	ΔEESC (ppbv)	May	June	July	August	September	October
V1 F1	345	−2.5	**−40.5** ± 10.8	**−38.6** ± 16.2	**−38.7** ± 31.6	−36.5 ± 43.6	−34.2 ± 43.2	−32.6 ± 34.0
V1 F4	345	−2.5	**−54.7** ± 12.8	**−46.2** ± 16.4	**−36.9** ± 29.8	−38.6 ± 45.8	−46.7 ± 48.6	**−62.9** ± 33.4
V1 F5	485	−2.5	**−66.2** ± 14.6	**−54.5** ± 16.2	**−26.2** ± 26.6	−32.0 ± 42.2	**−82.4** ± 46.4	**−102.5** ± 33.8
V2 F4	345	−2.5	**−52.8** ± 4.8	**−51.5** ± 12.2	**−52.5** ± 18.2	**−64.3** ± 23.0	**−70.3** ± 24.8	**−72.3** ± 20.6
Cl60	345	0	**−50.2** ± 11.4	**−57.6** ± 16.0	**−95.3** ± 35.0	**−99.8** ± 53.4	**−83.1** ± 52.4	**−54.1** ± 27.2

[a]10^{-3} K a^{-1}. Trends that are statistically significant at the 95% confidence level or higher are denoted in bold. Errors denote 2 standard deviations.

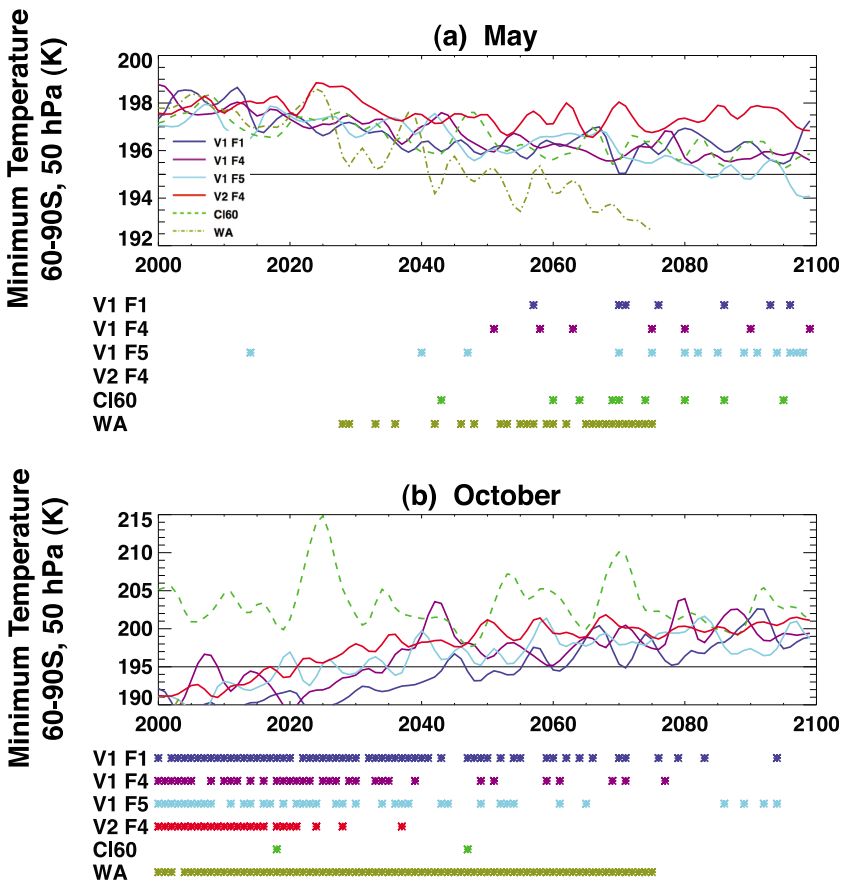

Figure 1. Minimum temperature poleward of 60°S at 50 hPa (K), between 2000 and 2099, in (a) May and (b) October. Shown are simulations V1 F1 (blue), V1 F4 (purple), V1 F5 (cyan), V2 F4 (red), Cl60 (green), and WA (brown). Solid lines denote "realistic future" simulations. Horizontal black lines denote 195 K. Three iterations of a 1-2-1 smoothing algorithm have been applied to all time series. Below each plot, symbols indicate years in which the minimum polar temperature at 50 hPa is equal to or below 195 K; note that, in May, there are no years that meet this criterion in the V2 F4 simulation.

below 195 K, for each month between May and October. A_{PSC} is a proxy for the 50 hPa "cold area" in which chemical ozone depletion can potentially occur, given the presence of sunlight. A_{PSC} = 0 when the minimum temperature in the polar region is greater than 195 K. Figure 1 shows time series of the minimum polar temperature at 50 hPa in May and October, after three iterations of a 1-2-1 smoothing algorithm (a Gaussian filter with a half-amplitude point of 6.67 years), and documents years in which the minimum temperature is 195 K or below (color-coded symbols). In May (Figure 1a), the polar minimum temperature remains above 195 K for the duration of the V2 F4 simulation, as wintertime lower stratospheric temperatures are generally warmer in the GEOS V2 CCM than in the GEOS V1 CCM [*Hurwitz et al.*, 2010]. In the "world avoided" simulation, minimum temperatures begin to drop below the chlorine activation threshold in the 2020s. In the GEOS V1 CCM "realistic future" simulations, there are minimum temperatures below 195 K and thus positive cold areas by the middle of the 21st century. In midwinter, minimum temperatures are generally less than 195 K. In October (Figure 1b), there are only 2 years when the minimum temperature is below 195 K in the Cl60 simulation. In the "realistic future" simulations, minimum polar temperatures generally increase, with fewer years below the 195 K threshold by the middle of the 21st century. Minimum temperatures are generally warmer in the V2 F4 simulation, since the breakup of the polar vortex, and the associated warming of the Antarctic stratosphere, occurs earlier in the GEOS V2 CCM than in the GEOS V1 CCM [*Hurwitz et al.*, 2010]. In WA, minimum temperatures remain below 190 K from 2004 through the end of the simulation and thus do not appear in the time series in Figure 1b.

[17] A_{PSC} trends at 50 hPa and their consistency among the various GEOS CCM simulations generally correspond with 50 hPa polar cap temperature trends for the 2000–2099 period. Monthly mean smoothed A_{PSC} time series for six GEOS CCM simulations are shown in Figure 2. The WA time series ends in 2075. In May (Figure 2a), the SH coverage by temperatures less than 195 K is relatively small (typically less than 2×10^6 km^2 or 1% hemispheric area coverage) but increases with time. The V1 F1, V1 F4, V1 F5, and Cl60 A_{PSC} trends are statistically significant (see Table 4). In the WA simulation, A_{PSC} magnitudes are much

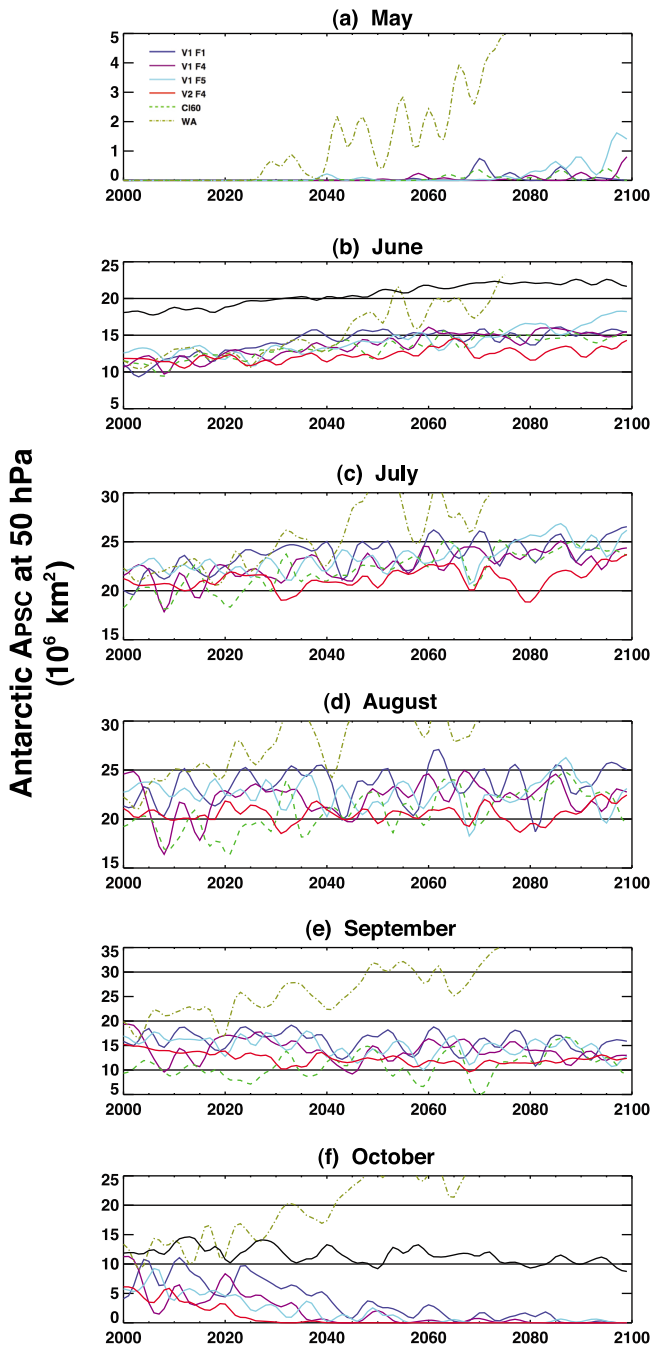

Figure 2. A_{PSC} at 50 hPa (10^6 km^2) between and 2000 and 2099. Shown are simulations V1 F1 (blue), V1 F4 (purple), V1 F5 (cyan), V2 F4 (red), Cl60 (green), and WA (brown). CMAM ensemble mean time series in (b) mid-June and (f) mid-October are shown in black. Solid lines denote "realistic future" simulations. Note the different vertical scales in each of the frames. Three iterations of a 1-2-1 smoothing algorithm have been applied to all time series.

larger than in the "realistic future" or Cl60 simulations. There are no cold areas in the V2 F4 simulation until June, as discussed above.

[18] In June (Figure 2b) and July (Figure 2c), A_{PSC} magnitudes are larger (10–25 × 10^6 km^2) and are similar among the "realistic future" and Cl60 simulations. A_{PSC} trends are positive in all of the simulations shown (Table 4). The GEOS V1 CCM simulations show similar increasing trends; different SST (V1 F1 versus V1 F4), greenhouse gas (V1 F4 versus V1 F5), and ODS scenarios (V1 F4 versus Cl60) do not affect the magnitude of the cold area trends. These trends are consistent with the change in Antarctic A_{PSC} during the 21st century in realistic future simulations in the CMAM in early June (ensemble mean trend of 4.90 ± 1.12 × 10^6 km^2 c^{-1}). In the V2 F4 simulation (red line), the A_{PSC} trend is smaller than the CMAM trend but positive and statistically significant nonetheless.

[19] In midwinter, the strong polar jet isolates large cold areas inside the polar vortex. In July and August (Figures 2c and 2d), cold areas cover roughly 10% of the total hemispheric area (~25 × 10^6 km^2) and are similar in the two versions of the GEOS CCM. In August, A_{PSC} trends are positive in the Cl60 and WA simulations; in the "realistic future" simulations, there are no apparent trends between 2000 and 2099.

[20] In spring, the cold area depends on the timing of the breakup of the Antarctic polar vortex. By October, sunlight has returned to the Antarctic polar region. In some winters, polar temperatures are close to or above the chlorine activation threshold (see Figure 1) and thus PSCs cannot form. However, in years when the vortex breakup has not yet occurred, A_{PSC} is large. In October (Figure 2f and Table 4), A_{PSC} trends diverge and correspond with the EESC trend in the respective simulation. Decreasing trends in the "realistic future" simulations are associated with the recovery of the ozone layer. The magnitude of the trend in V1 F1 is higher than in V1 F4 and V1 F5, suggesting that the choice of SST scenarios may impact 21st century polar stratospheric temperatures. A_{PSC} trends are smaller in both the V2 F4 simulation and in the CMAM ensemble mean (−2.82 ± 1.86 × 10^6 km^2 c^{-1}).

[21] A_{PSC} trends in the low chlorine (Cl60) and "world avoided" (WA) simulations are compared with trends in the realistic future simulations described above. These two simulations were forced with the same SST and greenhouse gas scenario (A1b) as for V1 F4 but with distinct ODS scenarios. In Cl60, stratospheric chlorine is too low for the formation of an ozone hole and temperatures are generally too high for the formation of PSCs in October (see Figure 1b). Thus, the October A_{PSC} trend is not significantly different from zero. In the "world avoided" case, cold areas increase from 2000 to 2049 (~28 × 10^6 km^2 c^{-1}, i.e., a 14 × 10^6 km^2 increase in cold area in 50 years). This trend is associated with the extreme ozone depletion possible under high chlorine levels [*Newman et al.*, 2009].

[22] At 10 hPa, well above the ozone hole, temperatures are much less influenced by changes in ODSs [*Shine et al.*, 2003]. Thus, temperature trends at 10 hPa reflect changes in SSTs and greenhouse gases, in the absence of ODS changes. T_{10hPa} trends are summarized in Table 3. Trends are negative in all simulations and in all months. Trends are all statistically significant in May, June, and July, with larger magnitudes than at 50 hPa. In September and October, variability is several times that seen in early winter, meaning that some spring trends are not statistically significant. In May, June, and October, V1 F5 trends are larger than the other realistic future simulations (though not at statistically significant levels), reflecting the larger change in CO_2 in the

Table 4. 2000–2099 Antarctic A_{PSC} Trends at 50 hPa[a]

	ΔCO_2 (ppmv)	ΔEESC (ppbv)	May (Figure 2a)	June (Figures 2b and 4a)	July (Figure 2c)	August (Figure 2d)	September (Figure 2e)	October (Figures 2f and 4b)
V1 F1	345	−2.5	**0.18** ± 0.18	**4.35** ± 1.60	**3.34** ± 1.80	1.45 ± 2.36	**−2.45** ± 2.60	**−9.93** ± 2.92
V1 F4	345	−2.5	**0.23** ± 0.16	**5.10** ± 1.46	**3.46** ± 1.98	1.65 ± 2.38	−1.76 ± 2.86	**−7.16** ± 2.44
V1 F5	485	−2.5	**0.67** ± 0.34	**5.10** ± 1.60	**3.53** ± 1.90	−0.19 ± 2.40	−2.72 ± 2.86	**−6.83** ± 2.32
V2 F4	345	−2.5	N/A	**2.10** ± 1.06	**1.53** ± 1.26	0.48 ± 1.34	**−2.37** ± 1.44	**−4.63** ± 1.34
Cl60	345	0	**0.19** ± 0.14	**4.46** ± 1.54	**5.55** ± 2.02	**4.86** ± 2.74	**3.15** ± 3.04	−0.03 ± 0.08

[a]10^6 km^2 c^{-1}. Trends that are statistically significant at the 95% confidence level or higher are denoted in bold. Errors denote 2 standard deviations.

late 21st century in the A2 GHG scenario than in A1b. The smallest cooling trends are seen in V1 F1, possibly reflecting the different SST and sea ice boundary conditions used in this simulation. As expected, differences between the ODS scenarios are less pronounced at 10 hPa, with comparable T_{10hPa} trends in the C160 and "realistic future" simulations in both autumn and spring.

[23] Cooling of the Antarctic lower stratosphere strengthens the meridional temperature gradient and, following the thermal wind balance, strengthens vertical wind shear and thus results in relatively stronger winds in the middle stratosphere. While peak jet speeds in the GEOS V1 CCM are biased high as compared with observations [*Pawson et al.*, 2008], the strength of the Antarctic jet increases at a statistically significant rate in all simulations. During the 2000–2099 period, zonal wind trends in June are small, positive (~4–5 m s^{-1} c^{-1} at 10 hPa, 60°S; see Figure 3), and consistent among the "realistic future" and Cl60 simulations. As noted by *Hurwitz et al.* [2010], the Antarctic jet is on average weaker in the GEOS V2 CCM than in the GEOS V1 CCM. During the 2000–2049, all simulations (including WA) show a similar increase in the strength of the Antarctic jet, though there is more variability in the magnitude of the zonal wind trends. In spring, in the "realistic future" simulations, the polar jet weakens in accordance with the relatively higher Antarctic temperatures predicted by the mid to late 21st century.

3.2. Trend Attribution

[24] In this section, statistical and radiative calculations are used to attribute early winter lower stratospheric cooling trends (decreasing T_{50hPa} and increasing A_{PSC}) to increased CO_2 concentrations and relate springtime temperature trends to changes in ODSs.

[25] First, 50 hPa A_{PSC} trends are analyzed via a multiple linear regression (similarly to the temperature trend analysis by *Stolarski et al.* [2010]). For each simulation and for each month, A_{PSC} trends are fitted to three factors known to affect polar stratospheric temperature: CO_2, EESC (at 1 hPa), and a proxy for polar downwelling (mean w^* between 10 and 30 hPa, 60°S–80°S) [see *Newman et al.*, 2001]. Figure 4 shows the results of the multiple linear regressions for 1975–2049 trends in four of the GEOS CCM simulations. The black dots show the actual A_{PSC} trends with error bars (as stated in Table 5). The trends fitted from the multiple linear regressions (gray dots) are in good agreement with the actual trends. Red dots show the CO_2-related contribution to each trend; blue dots show the EESC-related contribution; green dots show the contribution from polar downwelling.

[26] In June, increasing CO_2 accounts for positive A_{PSC} trends. The 1975–2049 period is ideal for trend attribution in the "realistic future" simulations, as the CO_2 and EESC time series are linearly independent (CO_2 increases monotonically, while EESC peaks in 2000). Figure 4a clearly shows that, in both V1 F2 and V1 F3, the CO_2 term accounts for positive A_{PSC} trends (see also Table 5). The roles of EESC and polar downwelling are small and are statistically distinct from the CO_2 contribution to the trends. In Cl60, the CO_2 term accounts for the positive (though not statistically significant) A_{PSC} trend; the EESC term is equal to zero. In WA, both increasing EESC and increasing CO_2 may contribute to the large, positive A_{PSC} trend. During the 2000–2099 period, A_{PSC} trends are positive and consistent among the four GEOS V1 CCM simulations (see Table 4). In Cl60, increasing CO_2 drives this trend, as the w^* term is small and there is no EESC contribution. However, in the "realistic future" simulations, CO_2 and EESC trends have the opposite sign (CO_2 increases monotonically throughout the 21st cen-

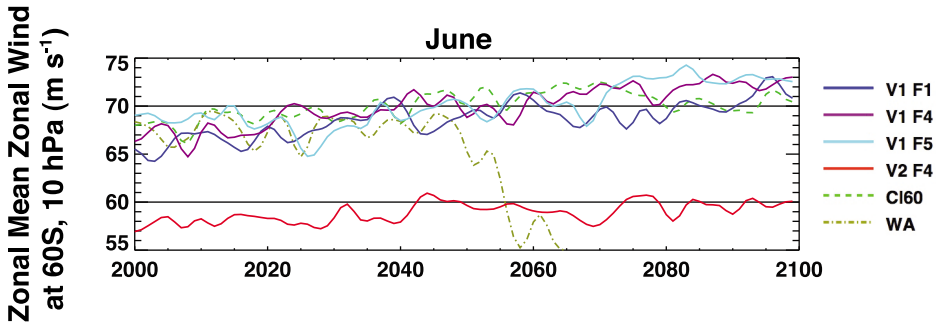

Figure 3. Time series of zonal mean zonal wind at 10 hPa, 60°S (m s^{-1}), between 2000 and 2099, in June. Shown are simulations V1 F1 (blue), V1 F4 (purple), V1 F5 (cyan), V2 F4 (red), Cl60 (green), and WA (brown). Solid lines denote "realistic future" simulations. Three iterations of a 1-2-1 smoothing algorithm have been applied to all time series.

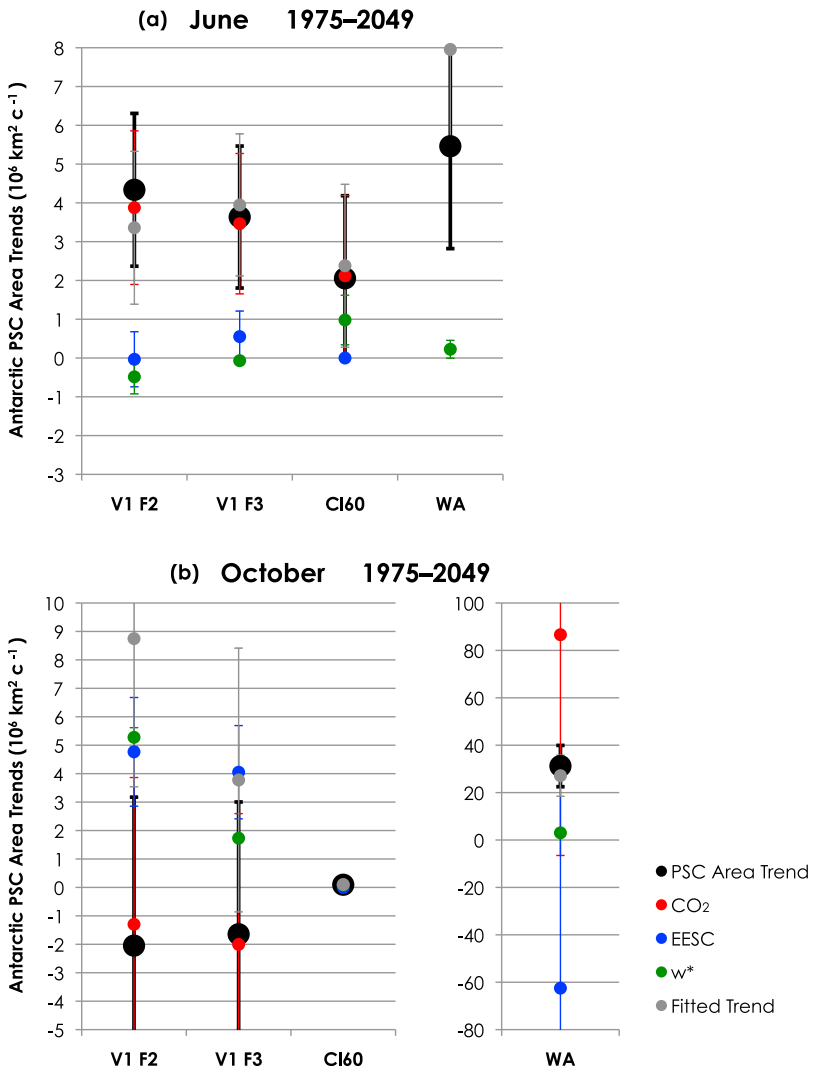

Figure 4. Results of the multiple linear regression of A_{PSC} trends at 50 hPa for the 1975–2049 period. Shown are regressions of the V1 F2 and V1 F3 A_{PSC} trends in (a) June and (b) October. The trends noted in Table 5 are shown in black. Fitted trends are shown as the gray dots. Red dots show the CO_2-related contribution; blue dots show the EESC-related contribution; green dots show the w^*-related (polar downwelling-related) contribution. Error bars denote ±2 standard deviations.

tury while EESC decreases monotonically). These circumstances imply that, in many cases, the CO_2 and EESC contributions to the A_{PSC} trends are not statistically distinct. Trend attribution for the "realistic future" simulations in the 2000–2099 period in June is unclear and is thus not shown.

[27] As expected, EESC changes account for the A_{PSC} trends in October (Figure 4b). The largest A_{PSC} trend occurs in WA; however, the CO_2 and EESC time series are nonorthogonal (both CO_2 and EESC increase monotonically between 1975 and 2075) and thus statistical trend attribution is not possible. EESC does not change in Cl60, accounting for the negligible A_{PSC} trends. For the 1975–2049 period, A_{PSC} trends in V1 F2 and V1 F3 are not statistically significant. For the 2000–2099 period, decreasing EESC trends

Table 5. 1975–2049 Antarctic A_{PSC} Trends at 50 hPa[a]

	ΔCO_2 (ppmv)	ΔEESC (ppbv)	May	June (Figure 5)	July	August	September	October
V1 F2	197	0.8	N/A	**4.34** ± 1.97	**4.63** ± 2.46	**3.64** ± 3.22	1.61 ± 4.00	−2.05 ± 5.22
V1 F3	197	0.8	0.05 ± 0.06	**3.63** ± 1.83	**3.38** ± 2.72	−0.84 ± 3.94	−4.45 ± 4.66	−1.65 ± 4.65
Cl60	197	0	N/A	2.05 ± 2.13	1.18 ± 3.08	1.43 ± 4.04	1.05 ± 4.04	0.09 ± 0.13
WA	197	28.2	**1.82** ± 1.22	**5.46** ± 2.64	**9.27** ± 3.68	**15.95** ± 5.18	**21.73** ± 6.76	**31.20** ± 8.71

[a]10^6 km^2 c^{-1}. Trends that are statistically significant at the 95% confidence level or higher are denoted in bold. Errors denote 2 standard deviations.

Table 6. June Polar Cap Temperature Differences at 50 hPa, Estimated From a Longwave Heating Rate of −2 K d^{-1}[a]

	ΔT From V1 F4 2000–2019 (K)	ΔT From V1 F5 2000–2019 (K)	ΔT V1 F5 − V1 F4 (K)
2000–2019	0	0	−0.13
2080–2099	−1.01	−1.06	−0.18
2000–2019 with 2080–2099 CO_2	−1.07	−0.97	
2000–2019 with 2080–2099 CH_4 and N_2O	−0.04	−0.12	
2000–2019 with 2080–2099 H_2O	−0.08	−0.06	
2000–2019 with 2080–2099 CFCs	0.00	−0.01	
2000–2019 with 2080–2099 O_3	0.01	0.22	

[a]Temperatures and longwave heating rates are calculated from an off-line radiative code, then fitted using a least squares technique. The top row of data shows temperature differences when 2000–2019 conditions are used in the radiative calculations. The second row of data shows temperature differences when 2080–2099 conditions are used in the radiative calculations. The third through seventh rows show temperature differences for 2000–2019 when 2080–099 values are substituted for one or more trace gas in the radiative calculations. Twenty year means are shown. Additional explanation is provided in the text.

in V1 F1, V1 F4, V1 F5, and V2 F4 correspond with negative trends in A_{PSC}, though in V1 F1 and V1 F4 the EESC and CO_2 contributions cannot be distinguished.

[28] Radiative flux calculations provide further evidence that increasing CO_2 drives the robust cooling trends seen in all simulations in early winter. Net radiative heating rates were calculated off-line [*Chou et al.*, 2001], using temperature and trace gas fields from the GEOS CCM simulations, and were converted to approximate longwave heating rates using the online modeled shortwave heating rates. This analysis focused on the polar cap region (60°S–90°S) at 50 hPa in June. Radiative calculations were made using output from each year of the V1 F4 and V1 F5 simulations. Differences between the 2000–2019 and 2080–2099 periods were used to assess predicted changes in longwave heating over the course of the 21st century.

[29] The radiative contributions of various trace gases to temperature changes between the early and late 21st century, for a given longwave heating rate, are shown in Table 6. For each case and for each simulation, a linear fit between longwave heating rates, obtained from the radiative calculations, and temperatures from the CCM simulations was used to estimate T_{50hPa} given a longwave heating rate of −2 K d^{-1}. Twenty year mean polar cap temperatures, expressed as differences from 2000 to 2019, are shown in the first two columns of Table 6. The second row of data shows that T_{50hPa} is lower in the late 21st century than in the early 21st century (see V1 F4 in Table 2). The polar cap temperature difference between 2000–2019 and 2080–2099 is ~1 K. The third through seventh rows of data show the contributions of various radiatively active gases (i.e., H_2O) to this temperature difference; specifically, temperature differences computed in cases when 2080–2099 concentrations of one or more trace gas was substituted for 2000–2019 concentrations in the radiative calculations. The temperature difference for the 2000−2019 case substituted with 2080–2099 CO_2 values is −1.07 K (−0.97 K) in V1 F4 (V1 F5), suggesting that that it is the change in CO_2 that drives the 21st century cooling trend in June. In V1 F4, temperature differences are less than 0.1 K in the cases of substitutions with 2080–2099 CH_4, N_2O, H_2O, CFC-11, CFC-12, CFC-22, and ozone values, implying that these gases make little or no contribution to 21st century cooling in the Antarctic lower stratosphere.

[30] Temperature differences between V1 F5 and V1 F4 are shown in the right-hand column of Table 6. During the 2000–2019 period, polar cap temperatures are on average cooler (0.13 K) in V1 F5 than in V1 F4. By the 2080–2099 period, CO_2 concentrations are higher in V1 F5 (forced by the A2 scenario for greenhouse gases) than in V1 F4 (A1b GHG scenario), enhancing radiative cooling. During 2080–2099, polar cap temperature differences between V1 F4 and V1 F5 are slightly larger (0.18 K) than those seen for the 2000–2019 period. The results of the off-line radiative calculations are similar in May and July (not shown).

[31] In summary, both multiple linear regression analysis and radiative calculations point to CO_2 as the primary driver of the robust June cooling (increasing A_{PSC}) trends; this result is expected, since an increasing trend in greenhouse gas concentrations is common to all of the simulations considered in this paper. Changes in stratospheric chlorine drive A_{PSC} trends in October.

3.3. Polar Ozone Trends

[32] In autumn and early winter, positive A_{PSC} trends, which suggest an increased potential for chemical ozone depletion in future, do not correspond with predicted ozone trends. Smoothed June ozone time series are shown in Figure 5a. In all but the WA simulation, Antarctic ozone at 50 hPa increases at a statistically significant rate between 2000 and 2099; this result is consistent with the relative increase in extratropical ozone by the late 21st century in GEOS CCM simulations, as noted by *Li et al.* [2009] and *Waugh et al.* [2009]. Ozone trends (Table 7) are consistent among the "realistic future" simulations and are smaller in the Cl60 simulation. Instantaneous ClO and HNO_3 fields, available on the first day of each month, respectively provide a "snapshot" view of chlorine activation and the presence of PSCs. In the realistic future simulations, there are positive ClO and HNO_3 trends in June (not shown). Thus, in the early winter, transport changes dominate over chemistry: Polar ozone increases despite lower temperatures and increased chlorine activation.

[33] In October (Figure 5b), polar ozone trends (no change in Cl60, decreasing in WA, increasing in the realistic future simulations) reflect trends in stratospheric chlorine and A_{PSC}, as discussed in the previous sections. Polar ozone trends are consistent among the four "realistic future" simulations.

4. Summary and Discussion

[34] The 21st century trends in polar stratospheric temperature and A_{PSC} were evaluated as a function of season. Robust cold area and temperature trends were found in the

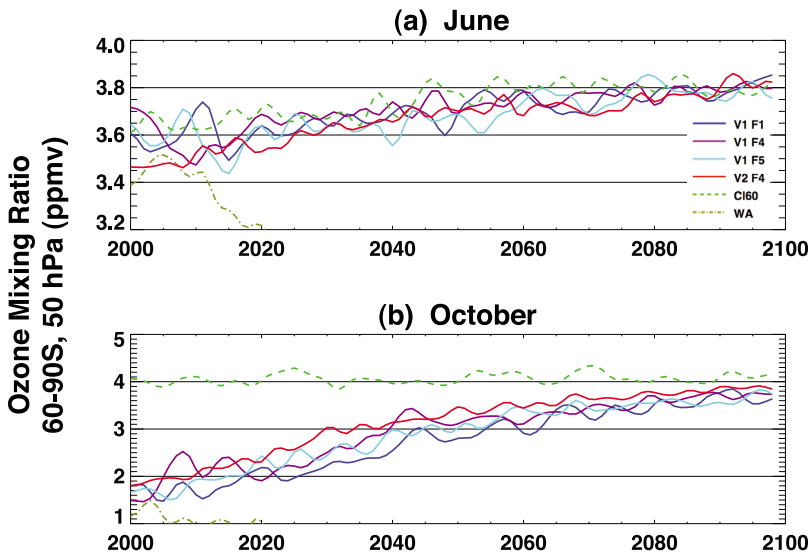

Figure 5. Time series of Antarctic ozone (60°S–90°S) at 50 hPa (ppmv), between 2000 and 2099, in (a) June and (b) October. Shown are simulations V1 F1 (blue), V1 F4 (purple), V1 F5 (cyan), V2 F4 (red), Cl60 (green), and WA (brown). Solid lines denote "realistic future" simulations. Three iterations of a 1-2-1 smoothing algorithm have been applied to all time series.

lower and middle Antarctic stratosphere, in both the autumn and early winter (May, June, and July) and in October. This study was the first to use a selection of greenhouse gas, ozone-depleting substance, and sea surface temperature scenarios to test the trend sensitivity to these parameters and to compare simulations of the 21st century in two versions of the GEOS CCM.

[35] In the autumn and early winter (May, June, and July) in the lower stratosphere, cooling trends were seen in all simulations. Both radiative calculations and multiple linear regressions confirmed that increasing CO_2 drove this cooling. The magnitudes of the early winter temperature trends (~1–3 K by 2100) were not affected by the choice of boundary conditions; however, stronger cooling would likely have been seen in a simulation forced by a sharper increase in CO_2. The Antarctic polar jet showed a corresponding strengthening. A_{PSC} trends in the GEOS V1 CCM "realistic future" simulations matched those found in another CCM [*Hitchcock et al.*, 2009; see Figure 2b and their Figure 3a] and were stronger than those seen in the GEOS V2 CCM simulation.

[36] In midwinter, A_{PSC} and T_{50hPa} did not change significantly throughout the 21st century. One exception was the "world avoided" simulation: large, positive A_{PSC} trends were found in the early and middle 21st century, due to extreme ozone depletion [*Newman et al.*, 2009].

[37] In October, the sign of the A_{PSC} trends corresponded with the respective trends in ODSs (and thus, in polar ozone depletion): positive in the "world avoided" simulation, no trend in the "low chlorine" simulation, and negative trends in the "realistic future" simulations; polar cap temperature trends had the opposite sign. A_{PSC} trends were larger in both versions of the GEOS CCM than in the CMAM ensemble mean (see Figure 2f), likely due to the relative cold bias in the lower stratosphere in the CMAM [*Eyring et al.*, 2006; *Hitchcock et al.*, 2009]. At 10 hPa, above the ozone hole, negative polar cap temperature trends in all simulations reflected increases in CO_2. By the late 21st century, there was stronger cooling in the A2 GHG scenario than in the A1b scenario; however, 2000–2099 temperature trends in the two scenarios were not statistically distinct.

[38] In the "realistic future" simulations, early winter ozone increased throughout the 21st century despite lower stratospheric cooling. Increased transport of ozone, due to the strengthening of the Brewer-Dobson circulation in future, overwhelmed the radiative and chemical changes that might have enhanced chemical ozone depletion. In October, polar ozone trends corresponded with the availability of stratospheric chlorine and were consistent with A_{PSC} trends. The magnitudes of the positive ozone trends were the same in all of the "realistic future" simulations. This result suggests that, for the subset of climate change scenarios tested

Table 7. 2000–2099 Polar Ozone Trends at 50 hPa[a]

	ΔCO_2 (ppmv)	ΔEESC (ppbv)	May	June (Figure 6a)	July	August	September	October (Figure 6b)
V1 F1	345	−2.5	**1.8** ± 0.6	**2.5** ± 0.8	**4.0** ± 1.0	**8.7** ± 1.8	**17.2** ± 3.6	**23.9** ± 5.2
V1 F4	345	−2.5	**1.7** ± 0.6	**2.4** ± 0.8	**3.9** ± 1.0	**8.6** ± 1.8	**16.0** ± 3.6	**21.2** ± 5.0
V1 F5	485	−2.5	**2.1** ± 0.8	**2.6** ± 0.8	**4.6** ± 1.2	**9.6** ± 2.2	**17.6** ± 3.8	**22.4** ± 4.8
V2 F4	345	−2.5	**2.7** ± 0.8	**3.4** ± 0.8	**5.2** ± 1.2	**10.2** ± 2.2	**18.0** ± 3.8	**21.6** ± 4.6
Cl60	345	0	**1.9** ± 0.6	**2.0** ± 0.8	**1.7** ± 0.8	**1.4** ± 1.0	1.1 ± 1.2	0.8 ± 1.4

[a]10^{-3} ppmv a^{-1}. Trends that are statistically significant at the 95% confidence level or higher are denoted in bold. Errors denote 2 standard deviations.

in this work, the choice of sea surface temperature and greenhouse gas scenarios has a negligible impact on future ozone trends in the polar lower stratosphere. Additional work will be required to quantify the impact of climate change, if any, on Antarctic ozone recovery.

[39] **Acknowledgments.** The authors thank J. E. Nielsen and L. D. Oman for running the GEOS CCM simulations, S. M. Frith for data processing, P. Hitchcock for providing CMAM output, E. R. Nash and E. Fleming for their assistance with the radiative flux calculations, R. S. Stolarski for assistance with the multiple linear regressions, M. A. Olsen for editing the manuscript, and NASA's MAP program for funding. M. M. Hurwitz was supported by an appointment to the NASA Postdoctoral Program at Goddard Space Flight Center, administered by Oak Ridge Associated Universities through a contract with NASA.

References

Akiyoshi, H., L. B. Zhou, Y. Yamashita, K. Sakamoto, T. Nagashima, M. Takahashi, J. Kurokawa, M. Takigawa, T. Imamura (2009), A CCM simulation of the breakup of the Antarctic polar vortex in the years 1980–2004 under the CCMVal scenarios, *J. Geophys. Res.*, *114*, D03103, doi:10.1029/2007JD009261.

Bloom, S., et al. (2005), Documentation and validation of the Goddard Earth-Observing System (GEOS) Data Assimilation System Version 4, *Tech. Rep. 104606*, *V26*, NASA, Greenbelt, Md.

Braesicke, P., M. M. Hurwitz, and J. A. Pyle (2006), The stratospheric response to changes in ozone and carbon dioxide as modeled with a GCM including parameterized ozone chemistry, *Meteorol. Z.*, *15*, 343–354.

Chou, M.-D., M. J. Suarez, X.-Z. Liang, and M. M.-H. Yan (2001), A thermal infrared radiation parameterization for atmospheric studies, NASA Tech. Memo, NASA/TM-2001-104606, vol. 19, 56 pp.

Collins, W. D., et al. (2006), The community climate system model version 3 (CCSM3), *J. Clim.*, *19*, doi:10.1175/JCLI3761.1.

Efron, B. (1979), Bootstrap methods: another look at the jackknife, *Ann. Stat.*, *7*, 1–26.

Eyring, V., et al. (2006), Assessment of temperature, trace species, and ozone in chemistry-climate model simulations of the recent past, *J. Geophys. Res.*, *111*, D22308, doi:10.1029/2006JD007327.

Eyring, V., et al. (2007), Multimodel projections of stratospheric ozone in the 21st century, *J. Geophys. Res.*, *112*, D16303, doi:10.1029/2006JD008332.

Hitchcock, P., T. G. Shepherd, and C. McLandress (2009), Past and future conditions for polar stratospheric cloud formation simulated by the Canadian Middle Atmosphere Model, *Atmos. Chem. Phys.*, *9*, 483–495.

Hurwitz, M. M., P. A. Newman, F. Li, L. D. Oman, O. Morgenstern, P. Braesicke, and J. A. Pyle (2010), Assessment of the breakup of the Antarctic polar vortex in two new chemistry-climate models, *J. Geophys. Res.*, *115*, D07105, doi:10.1029/2009JD012788.

Intergovernmental Panel on Climate Change (IPCC) (2002), *Climate Change 2001: The Scientific Basis: Contribution of Working Group 1 to the Third Assessment Report of the Intergovernmental Panel on Climate Change*, edited by J. T. Houghton et al., Cambridge Univ. Press, New York.

Johns, T. C., et al. (2006), The new Hadley Centre Climate Model (HadGEM1): Evaluation of coupled simulations, *J. Clim.*, *19*, 1327–1353.

Kawa, S. R., et al. (1997), Activation of chlorine in sulfate aerosol as inferred from aircraft observations, *J. Geophys. Res.*, *102*(D3), 3921–3933, doi:10.1029/96JD01992.

Li, F., R. S. Stolarski, P. A. Newman (2009), Stratospheric ozone in the post-CFC era, *Atmos. Chem. Phys.*, *9*, 2207–2213.

Manzini, E., B. Steil, C. Bruhl, M. A. Giorgetta, and K. Kruger (2003), A new interactive chemistry-climate model: 2. Sensitivity of the middle atmosphere to ozone depletion and increase in greenhouse gases and implications for recent stratospheric cooling, *J. Geophys. Res.*, *108*(D14), 4429, doi:10.1029/2002JD002977.

Newman, P. A., E. R. Nash, and J. E. Rosenfield (2001), What controls the temperature of the Arctic stratosphere during the spring?, *J. Geophys. Res.*, *106*(D17), 19,999–20,010, doi:10.1029/2000JD000061.

Newman, P. A., S. R. Kawa, and E. R. Nash (2004), On the size of the Antarctic ozone hole, *Geophys. Res. Lett.*, *31*, L21104, doi:10.1029/2004GL020596.

Newman, P. A., et al. (2009), What would have happened to the ozone layer if CFCs had not been regulated?, *Atmos. Chem. Phys.*, *9*, 2113–2128.

Oman, L. D., D. W. Waugh, S. Pawson, R. S. Stolarski, and P. A. Newman (2009), On the influence of anthropogenic forcings on changes in the stratospheric mean age, *J. Geophys. Res.*, *114*, D03105, doi:10.1029/2008JD010378.

Oman, L. D., D. W. Waugh, S. R. Kawa, R. S. Stolarski, A. R. Douglass, and P. A. Newman (2010), Mechanisms and feedbacks causing changes in upper stratospheric ozone in the 21st century, *J. Geophys. Res.*, *115*, D05303, doi:10.1029/2009JD012397.

Pawson, S., R. S. Stolarski, A. R. Douglass, P. A. Newman, J. E. Nielsen, S. M. Frith, and M. L. Gupta (2008), Goddard Earth-Observing System chemistry-climate model simulations of stratospheric ozone-temperature coupling between 1950 and 2005, *J. Geophys. Res.*, *113*, D12103, doi:10.1029/2007JD009511.

Ramaswamy, V., et al. (2001), Stratospheric temperature trends: Observations and model simulations, *Rev. Geophys.*, *39*(1), 71–122, doi:10.1029/1999RG000065.

Ramaswamy, V., et al. (2006), Anthropogenic and natural influences in the evolution of lower stratospheric cooling, *Science*, *311*, 1138–1141.

Randel, W. J., et al. (2009), An update of observed stratospheric temperature trends, *J. Geophys. Res.*, *114*, D02107, doi:10.1029/2008JD010421.

Rex, M., R. J. Salawitch, P. von der Gathen, N. P. R. Harris, M. P. Chipperfield, and B. Naujokat (2004), Arctic ozone loss and climate change, *Geophys. Res. Lett.*, *31*, L04116, doi:10.1029/2003GL018844.

Rex, M., et al. (2006), Arctic winter 2005: Implications for stratospheric ozone loss and climate change, *Geophys. Res. Lett.*, *33*, L23808, doi:10.1029/2006GL026731.

Rienecker, M. M., et al. (2008), The GEOS-5 Data Assimilation System—Documentation of Versions 5.0.1, 5.1.0 and 5.2.0. Tech. Rep. Series on Global Modeling and Data Assimilation, 27.

Shine, K. P., et al. (2003), A comparison of model-simulated trends in stratospheric temperatures, *Q. J. R. Meteorol. Soc.*, *129*, 1565–1588.

Stolarski, R. S., A. R. Douglass, P. A. Newman, S. Pawson, and M. R. Schoeberl (2010), Relative contribution of greenhouse gases and ozone-depleting substances to temperature trends in the stratosphere: A chemistry-climate model study, *J. Clim.*, *23*, 28–42, doi:10.1175/2009JCLI2955.1.

Tilmes, S., D. E. Kinnison, R. R. Garcia, R. Muller, F. Sassi, D. R. Marsh, and B. A. Boville (2007), Evaluation of heterogeneous processes in the polar lower stratosphere in the Whole Atmosphere Community Climate Model, *J. Geophys. Res.*, *112*, D24301, doi:10.1029/2006JD008334.

Waugh, D. W, L. D. Oman, S. R. Kawa, R. S. Stolarski, S. Pawson, A. R. Douglass, P. A. Newman, and J. E. Nielsen (2009), Impacts of climate change on stratospheric ozone recovery, *Geophys. Res. Lett.*, *36*, L03805, doi:10.1029/2008GL036223.

World Meteorological Organization (WMO) (2003), Scientific assessment of ozone depletion: 2002, Global Ozone Res. And Monitor. Proj. Rep. 47, Geneva.

M. M. Hurwitz, NASA Postdoctoral Program, NASA Goddard Space Flight Center, Greenbelt, MD 20771, USA. (margaret.m.hurwitz@nasa.gov)

P. A. Newman, NASA Goddard Space Flight Center, Code 613.3, Greenbelt, MD 20771, USA.